JOURNAL OF Materials CHEMISTRY

Oxygen stoichiometry and structural properties of $La_{1-x}A_xMnO_{3\pm\delta}$ (A = Ca or Sr and $0 \leqslant x \leqslant 1$)

Lisbeth Rørmark,[a] Kjell Wiik,[a] Svein Stølen[b] and Tor Grande*[a]

[a]*Department of Chemistry, Norwegian University of Science and Technology, N-7491 Trondheim, Norway. E-mail: tor.grande@chembio.ntnu.no*
[b]*Department of Chemistry, University of Oslo, N-0315 Oslo, Norway*

Received 19th April 2001, Accepted 15th November 2001
First published as an Advance Article on the web 12th February 2002

Oxygen non-stoichiometry, structural properties, and phase relations in Ca and Sr substituted $LaMnO_{3\pm\delta}$ were studied by means of thermal analysis, X-ray diffraction, and iodometric titration. Hexagonal α-$SrMnO_{3-\delta}$ and $LaMnO_{3\pm\delta}$ perovskite are only partly miscible. Room temperature metastable $La_{1-x}Sr_xMnO_{3\pm\delta}$ solid solutions, prepared by quenching from high temperatures where there is complete solid solubility between cubic β-$SrMnO_{3-\delta}$ and $LaMnO_{3\pm\delta}$ perovskite, have rhombohedral, tetragonal or cubic symmetry dependent on the Sr content. Orthorhombic $LaMnO_{3+\delta}$ and $CaMnO_{3-\delta}$ form a stable $La_{1-x}Ca_xMnO_{3\pm\delta}$ solid solution in the whole composition region. The unit cell volume of $La_{1-x}Sr_xMnO_{3\pm\delta}$ and $La_{1-x}Ca_xMnO_{3\pm\delta}$ solid solutions is reduced with decreasing La-content mainly due to the correlated change in average oxidation state from Mn^{3+} to Mn^{4+}. The oxygen stoichiometry changes from cation deficient (oxygen excess) at high La-content to oxygen deficiency at low La-content. The enthalpy of the phase transitions of $CaMnO_{3-\delta}$ and the transition from α-$SrMnO_3$ (hexagonal) to β-$SrMnO_{3-\delta}$ (perovskite) were obtained by differential thermal analysis. Finally, the physical appearance of first order phase transition between different perovskite-related structures is analysed in terms of the Gibbs phase rule. First order transitions between different structures of a ternary oxide $ABO_{3-\delta}$ become two-phase regions in a quasi-binary system like $ABO_{3-\delta}$–$A'BO_{3-\delta}$.

Introduction

The substitution level of A in $La_{1-x}A_xMnO_{3\pm\delta}$(A = Sr or Ca) strongly influences the magnetic and electronic properties as well as the ionic conductivity, and a large number of studies have reported various materials properties as a function of substitution level.[1–7] However, the phase relations in the systems $LaMnO_3$–$SrMnO_3$ and $LaMnO_3$–$CaMnO_3$ are still a matter of discussion, and so is the variation in structural properties with oxygen non-stoichiometry for compositions ranging from pure $LaMnO_{3+\delta}$ to $AMnO_{3-\delta}$ (A = Ca or Sr).

The crystal structure of perovskite $LaMnO_{3+\delta}$ is determined by the formal oxidation state of Mn.[8,9] $LaMnO_{3+\delta}$ ($\delta < 0.1$) is orthorhombic, while for $\delta > 0.1$($> 44\%$ Mn^{4+}) $LaMnO_{3+\delta}$ is rhombohedral.[8] $LaMnO_{3+\delta}$ quenched in air from below 1000 °C is orthorhombic and above 1000 °C rhombohedral.[10–12] A two-phase mixture of rhombohedral and orthorhombic $LaMnO_{3+\delta}$ was observed in materials quenched from 1000 °C in air.[10,11] Orthorhombic $LaMnO_{3.00}$ (ORT1) transforms to a second orthorhombic (ORT2) phase at around 700 K[8,9,13] and further to a rhombohedral structure at 820 K. Both transitions are connected with discontinuous volume contractions and are first order in nature. The enthalpy associated with the transitions and the unit cell parameters of the three phases are dependent on the oxidation state of Mn in $LaMnO_{3+\delta}$ (δ). With increasing oxidation state of Mn the ORT1–ORT2 phase transition temperature is suppressed from about 700 K ($\delta = 0$) to below 77 K ($\delta = 0.073$).[8] Rhombohedral $LaMnO_{3+\delta}$ is stable up to 1000 °C in oxygen partial pressures between 1 and 10^{-5} atm.[14] At lower partial pressures the two orthorhombic structures were observed below 700 °C. The defect chemistry of $LaMnO_{3\pm\delta}$ is unique and both oxygen deficient and oxygen excess materials are stable. The oxygen excess $LaMnO_{3+\delta}$ is in reality cation deficient and thus more correctly described as $La_{1-y}Mn_{1-y}O_3$.[15]

Calcium substituted lanthanum manganese oxide, $La_{1-x}Ca_xMnO_{3\pm\delta}$ (LCM), is either rhombohedral or orthorhombic dependent on substitution level and partial pressure of O_2. At low substitution levels, $x \leqslant 0.14$, and high oxygen content, LCM is rhombohedral with space group $R\bar{3}c$.[1] For $0.2 \leqslant x \leqslant 1.0$ LCM is orthorhombic with space group *Pnma*.[2,5,16,17]

The crystal structure of perovskite $CaMnO_3$ in air is orthorhombic below 896 °C, tetragonal between 896 and 913 °C, and cubic above 913 °C.[18] The corresponding phase transitions were also observed for $Ca_{1-x}La_xMnO_{3-\delta}$ ($x = 0.05$ and 0.1), but were not observed for $x > 0.1$.[19] Orthorhombic $CaMnO_3$ can be topotactically reduced at about 300 °C to $CaMnO_{2.5}$, an orthorhombic perovskite-related phase with ordered oxygen defects.[20] The reoxidation of $CaMnO_{2.5}$ is rapid in air at temperatures as low as 300 °C.[20]

Strontium substituted lanthanum manganese oxide, $La_{1-x}Sr_xMnO_{3\pm\delta}$ (LSM), has been found to crystallise in rhombohedral, orthorhombic, tetragonal and cubic structures. LSM prepared in air and slowly cooled is rhombohedral for $0.0 \leqslant x \leqslant 0.5$.[21–23] $La_{0.9}Sr_{0.1}MnO_{3+\delta}$ is rhombohedral up to 1000 °C in 1–10^{-15} atm O_2.[15] Rhombohedral $La_{0.7}Sr_{0.3}MnO_{3+\delta}$ was stable up 900 °C in 1–10^{-10} atm O_2, but transformed to the cubic structure above 900 °C. Orthorhombic LSM with low Sr content is stabilised by quenching from high temperatures or reducing conditions.[21,22,24,25] Single phase LSM with $x \geqslant 0.6$[3] is only obtained at high temperatures due to the low solubility of hexagonal α-$SrMnO_3$, which does not have the perovskite structure.[26] Kikuchi *et al.*[3] found that after annealing in oxygen, materials with $0.5 \leqslant x \leqslant 0.6$ were tetragonal, while materials with $0.7 \leqslant x \leqslant 1.0$ were cubic.

While Mn-O_6 octahedra share corners in perovskite β-$SrMnO_{3-\delta}$, they share faces in hexagonal α-$SrMnO_3$.[26] α-$SrMnO_{2.89}$ transforms to β-$SrMnO_{2.74}$ at about 1400 °C in air.[26] On further heating β-$SrMnO_{3-\delta}$ becomes more oxygen deficient until it melts at 1740 °C.[26] The temperature for the α–β

 DOI: 10.1039/b103510j

$SrMnO_{3-\delta}$ transition was found to decrease with decreasing partial pressure of oxygen.[27] β-$SrMnO_{3-\delta}$ quenched from 1525 °C in air had an orthorhombic structure, and cubic $SrMnO_3$ was easily obtained by oxidation at 300 °C in air.[26] The phase transition from metastable β-$SrMnO_3$ to the stable α-$SrMnO_3$ was observed at about 800 °C.[26]

Cherepanov *et al.*[28] have studied the phase equilibria in the pseudo binary system $LaMnO_3$–$SrMnO_3$ at 1100 °C and various partial pressures of oxygen ($0.21\ \text{atm} \geqslant P_{O_2} \geqslant 10^{-14}$ atm). The solubility of α-$SrMnO_{3-\delta}$ in $La_{1-x}Sr_xMnO_{3-\delta}$ perovskite was $x = 0.38$ in air. Decreasing the partial pressure of oxygen increases the solubility limit to $x = 0.7$ at $P_{O_2} = 10^{-9}$ atm, while the solubility decreases again on further reduction of the partial pressure of oxygen. Majewski *et al.*[29] have reported quasi binary phase diagrams for the systems $LaMnO_3$–$SrMnO_3$ and $LaMnO_3$–$CaMnO_3$. They found that both systems show a miscibility gap at intermediate La/Sr and La/Ca ratios below about 1400 °C in air. The La-rich $SrMnO_{3-\delta}$ phase was found to crystallise in an orthorhombic distorted hexagonal modification as found for pure α-$SrMnO_{3-\delta}$ between 1222 and 1400 °C.[26] Sr- and Ca-rich $LaMnO_{3-\delta}$ and La-rich $CaMnO_{3-\delta}$ all had a perovskite-type structure. The SEM and XRD data provided for the two-phase regions by the authors are unclear and do not strengthen their conclusion. The two-phase region in the LSM system can be understood in terms of the immiscibility of hexagonal α-$SrMnO_3$ and Sr-substituted $LaMnO_3$ perovskite. The two-phase region in LCM has not been supported by other studies.

We have started a program to investigate the thermodynamic properties of the solid solutions $La_{1-x}A_xMnO_{3\pm\delta}$ (A = Ca or Sr, $0 \leqslant x \leqslant 1$). In the present paper we report on the oxygen non-stoichiometry and unit cell parameters in these systems. Phase relations in the two systems are also discussed. Furthermore, measurements of the enthalpies of oxidation of $Ca_2Mn_2O_5$, Ca_2MnO_4 and $Sr_2Mn_2O_5$ by *in situ* adiabatic calorimetry,[30] the heat capacities of $CaMnO_{3-\delta}$ and $SrMnO_{3-\delta}$ by adiabatic calorimetry,[31] and finally the enthalpies of formation of $La_{1-x}A_xMnO_{3\pm\delta}$ by high temperature solution calorimetry[32] are reported in separate papers.

Experimental procedure

Synthesis

LCM and LSM powders with 20, 40, 60, and 80 mol% substitution were synthesised by the amorphous citrate process. Pure $LaMnO_{3+\delta}$, $CaMnO_3$, and $SrMnO_3$ were prepared by the EDTA precursor method. $La(NO_3)_3{\cdot}6H_2O$(> 99.0%, Merck), $Ca(NO_3)_2{\cdot}H_2O$ (>99.0%, Merck), $Sr(NO_3)_2$ (>99,0% Merck), and $Mn(NO_3)_2{\cdot}4H_2O$ (>98.5%, Merck) were used in the two synthesis routes. The nitrates were heat treated between 700 °C and 1100 °C to determine the exact amount of crystal water.

In the amorphous citrate process the citric acid (>99.5%, Merck) was dissolved in 20 ml of ion-exchanged water, then the stoichiometric amounts of nitrates were dissolved in the acidic solution. The solution was heated on a hot plate to 80 ± 3 °C. The solution was continuously stirred at 80 °C until viscous foam was formed. The foam was dried overnight at 150–200 °C.

In the EDTA method stoichiometric amounts of nitrates were dissolved in ion-exchanged water, then an EDTA (ethylendiamine–tetraacetic acid, >99.7%, Sigma) solution (0.8 M and pH 8–9) was added. The final solution was heated on a hot plate to 80 ± 3 °C. The solution was continuously stirred at 80 °C until a gel was formed. The pH was controlled during heating, and NH_3 (concentrated, 15 M) was added to keep the pH at 7–11 depending on the type of ions in the solution. The gel was dried overnight at 150–200 °C.

The dried precursors from the two synthesis routes were crushed, and the powders were then fired at approximately 500 °C to remove all the organic matter. To obtain phase pure materials the powders were heat-treated at varying temperatures, see Table 1. In order to achieve the metastable perovskite $SrMnO_{3-\delta}$, hexagonal $SrMnO_{3.0}$ powder was annealed at 1525 °C in air for 2 h and subsequently air quenched to room temperature. This gave a cylindrical body where the outer surface was hexagonal (due to oxidation during cooling), while the interior of the cylinder was pure perovskite $SrMnO_{3-\delta}$. These two phases were easily separated due to colour differences, and all further handling and measurements were performed on the metastable perovskite phase of $SrMnO_3$. The crystal symmetry of the perovskite $SrMnO_{3-\delta}$ was confirmed by X-ray diffraction.

Several pellets of the precursor of $La_{0.2}Sr_{0.8}MnO_{3\pm\delta}$ were heat-treated at temperatures between 1100 and 1350 °C for 60 h before being quenched in air. This was done to study the phase behaviour of $La_{0.2}Sr_{0.8}MnO_{3\pm\delta}$ as a function of temperature.

Characterisation

Lattice cell dimensions of the materials were determined by X-ray diffraction (SIEMENS D5005, Siemens Germany) using Cu-K_α radiation. Silicon was used as an internal standard in order to determine the unit cell parameters. Powder X-ray diffraction was also used to study the phase relations in the systems $LaMnO_3$–$CaMnO_3$ and $LaMnO_3$–$SrMnO_3$.

The oxygen stoichiometry of the materials was determined by thermogravimetry (Perkin Elmer TGS2 or TGA 7, Perkin-Elmer Corporation, USA) and iodometry. In the thermogravimetric measurements samples of 35–80 mg were used. The weight change from room temperature to 700 °C and from 700–1000 °C in steps of 50 °C was recorded, in both synthetic air and N_2 ($P_{O_2} = 3\times10^{-6}$ atm). The measurements were corrected for drift due to the change in buoyancy with temperature. The corrected weight changes were used to calculate the oxygen stoichiometry at the different temperatures, using the results

Table 1 Heat treatment for the materials

Sample	Starting condition	Heat treatment	Atmosphere	Air quenched
$LaMnO_{3+\delta}$	Precursor	1000 °C/96 h + 1100 °C/5 h	Air	—
$LaMnO_{3.00}$	$LaMnO_{3+\delta}$	900 °C/198 h	N_2	—
LCM, Ca = 0.2	Precursor	1000 °C/96 h	Air	—
LCM, Ca = 0.4	Precursor	1000 °C/96 h	Air	—
LCM, Ca = 0.6	Precursor	1000 °C/96 h	Air	—
LCM, Ca = 0.8	Precursor	1000 °C/96 h	Air	—
$CaMnO_3$	Precursor	1100 °C/72 h + 1200 °C/96 h	Air	—
LSM, Sr = 0.2	Precursor	1150 °C/120 h	Air	—
LSM, Sr = 0.4	Precursor	1150 °C/60 h	Air	—
LSM, Sr = 0.6	Precursor	1400 °C/24 h	Air	V
LSM, Sr = 0.8	Precursor	1400 °C/24 h	Air	V
α-$SrMnO_3$ (hex.)	Precursor	1100 °C/72 h	Air	—
β-$SrMnO_3$ (per.)	α-$SrMnO_3$	1525 °C/2 h	Air	V

Table 2 Unit symmetry, oxygen stoichiometry, and unit cell parameters of the materials

Sample	Structure	a/Å	b/Å	c/Å	a_R/Å	α/°	V/Å^3
$LaMnO_{3.16}$	Hexagonal/Rhombohedral	5.5248(4)		13.331(1)	5.470	60.663	58.733
$LaMnO_{3.03}$	Orthorhombic	5.538(1)	7.712(1)	5.6905(7)	—	—	60.756
$La_{0.8}Ca_{0.2}MnO_{3.07}$	Orthorhombic	5.473(4)	7.740(4)	5.497(3)	—	—	58.212
$La_{0.6}Ca_{0.4}MnO_{3.00}$	Orthorhombic	5.445(1)	7.685(2)	5.456(2)	—	—	57.071
$La_{0.4}Ca_{0.6}MnO_{3.00}$	Orthorhombic	5.398(3)	7.599(3)	5.402(2)	—	—	55.404
$La_{0.2}Ca_{0.8}MnO_{3.00}$	Orthorhombic	5.332(3)	7.549(4)	5.335(3)	—	—	53.678
$CaMnO_{3.00}$	Orthorhombic	5.274(3)	7.467(5)	5.277(2)	—	—	51.952
$La_{0.8}Sr_{0.2}MnO_{3.06}$	Hexagonal/Rhombohedral	5.5155(2)	—	13.3543(7)	5.473	60.512	58.637
$La_{0.6}Sr_{0.4}MnO_{3.00}$	Hexagonal/Rhombohedral	5.49(4)	—	13.35(1)	5.463	60.293	58.027
$La_{0.4}Sr_{0.6}MnO_{3.00}$	Tetragonal	7.681(1)	—	7.736(2)	—	—	57.041
$La_{0.2}Sr_{0.8}MnO_{3.00}$	Cubic	3.8281(1)	—	—	—	—	56.098
$SrMnO_{3.00}$	Cubic	3.8061(1)	—	—	—	—	55.138
$SrMnO_{2.98}$	Cubic	3.8073(5)	—	—	—	—	55.189
$SrMnO_{3-\delta}$	Hexagonal	5.4516(6)	—	9.091(1)	—	—	58.494

from iodometric titration. The oxygen stoichiometry of $CaMnO_{3-\delta}$ and $SrMnO_{3-\delta}$ was also determined by TG. Samples of calcium and strontium manganite were heated to 700 and 500 °C in air, respectively, where they became stoichiometric. The oxygen stoichiometry of the materials was then calculated from the increase in mass due to oxidation.

The oxygen stoichiometry of the materials at room temperature was measured by iodometric titration.[33] The powders used for these measurements were slowly cooled (1 °C min^{-1}) from 700 °C to room temperature prior to analysis. The obtained data were used as a reference for the thermogravimetric analysis.

Iodometric titration was performed on 10–30 mg of sample. The sample was weighed out in a round-necked vessel. An excess of potassium iodide (KI) and *ca.* 10–20 ml distilled degassed water were added. The solution was made acidic by the addition of a few droplets of 0.1 M hydrochloric acid, then the vessel was closed and heated in order to dissolve the sample. The solution was cooled and titrated with standardised sodium thiosulfate (0.01 M). Starch was used as an indicator. This gave the mean valency of manganese, and the amount of oxygen in the materials was then calculated.

Heat effects (endothermic/exothermic) for some compositions were measured by differential thermal analysis (DTA) (STA 449 C, Jupiter, TG/DSC sample holder, NETZSCH-Gerätebau GmbH, Germany). Powders were analysed from room temperature to 1200 or 1350 °C in flowing air or N_2 with a heating and cooling rate of 10 °C min^{-1}. Temperature and sensitivity calibrations were performed according to the recommendation of the supplier, by measuring the temperature and enthalpy of melting of Sn, Ag, Au, CsCl, Al, Zn, and Cu.

Results

The LCM system ($0.0 \leqslant x \leqslant 1.0$)

Unit cell dimensions. The crystal system and unit cell dimensions of the materials are given in Table 2. $LaMnO_{3-\delta}$ was synthesised with two different oxygen stoichiometries. The crystal structure of rhombohedral $LaMnO_{3.16}$ was consistent with literature.[13,15] Reduction of $LaMnO_{3.16}$ in N_2 gave orthorhombic $LaMnO_{3.03}$ with unit cell dimensions in good accord with published data.[13,34] $La_{1-x}Ca_xMnO_{3\pm\delta}$ (x = 0.2, 0.4, 0.6, 0.8, and 1.0) were indexed as orthorhombic, which is also consistent with the literature.[2,16,17,35]

The unit cell dimensions of the orthorhombic LCM ($0.0 \leqslant x \leqslant 1.0$) materials are plotted in Fig. 1. The unit cell dimensions decrease with an increasing substitution level of Ca. The unit cell volume of the materials with stoichiometric oxygen content (LCM with x = 0.4, 0.6, 0,8, and 1.0) shows a near linear correlation with the degree of substitution, while the oxygen excess materials $LaMnO_{3.03}$ and $La_{0.8}Ca_{0.2}MnO_{3.07}$ deviate from this linear relationship.

Phase relations. $La_{1-x}Ca_xMnO_{3\pm\delta}$ (x = 0.0, 0.5, 0.8, 0.9, and 1.0) was studied by DTA/TGA. No evidence of a miscibility gap was observed for the LCM system in contradiction to the study by Majewski *et al.*[29] $CaMnO_{3-\delta}$ gave endothermic peaks at 904 ± 2 and 923 ± 2 °C on heating to 1200 °C in air, and exothermic peaks at 906 ± 2 and 925 ± 2 °C on cooling, respectively see Fig. 2. The energy involved in the two transitions were 1.7 and 0.3 kJ mol^{-1} for the first and second transition, respectively. Only the first phase transition was observed for $La_{0.1}Ca_{0.9}MnO_{3\pm\delta}$ at 914 ± 2 °C on heating, and on cooling an exothermic peak appeared at 922 ± 2 °C (Fig. 2). The phase transitions of both $La_{0.1}Ca_{0.9}MnO_{3\pm\delta}$ and $CaMnO_{3-\delta}$ are correlated with a change in the oxidation state of Mn (Fig. 2). The oxygen stoichiometry of $CaMnO_{3-\delta}$ showed no hysteresis at a heating and cooling rate of 10 °C min^{-1}, while significant lower oxygen content was observed for $La_{0.9}Ca_{0.1}MnO_{3-\delta}$ during cooling due to slow oxidation. No endothermic or exothermic peaks were observed for $La_{0.2}Ca_{0.8}MnO_3$ and $La_{0.5}Ca_{0.5}MnO_3$. The reduction of $La_{0.2}Ca_{0.8}MnO_{3-\delta}$ initiated at about 930 °C in air.

No evidence for phase transitions was observed by DTA/TGA during heating of $LaMnO_{3.16}$ to 1350 °C in air. The

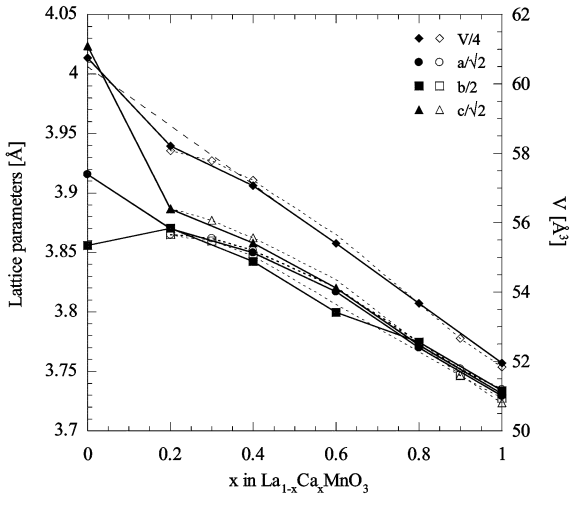

Fig. 1 Pseudocubic unit cell dimensions for the orthorhombic LCM system. Filled symbols with solid lines are results from this work. Open symbols with dotted lines are literature data.[2,17] $La_{1-x}Ca_xMnO_3$ with x = 0.4, 0.6, 0.8, and 1.0 are stoichiometric, while materials with x = 0.0 and 0.2 have oxygen excess. The dashed line shows the linear relationship between the unit cell volume and the degree of substitution for stoichiometric samples.

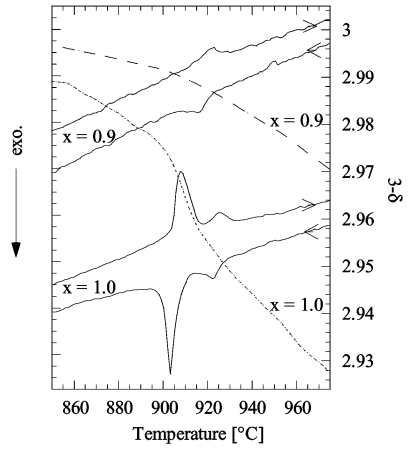

Fig. 2 DTA (solid lines) and TGA (dashed and dotted line) curves for $La_{1-x}Ca_xMnO_{3-\delta}$ with $x = 0.9$ and 1.0 in air. The heating rate was 10 °C h^{-1}.

reduction of $LaMnO_{3.16}$ initiated at 700 °C. The oxygen stoichiometry was reduced to $LaMnO_{3.04}$ at 1350 °C, which is considerably less than the oxygen stoichiometry at the rhombohedral to orthorhombic phase transition taking place at room temperature.[8]

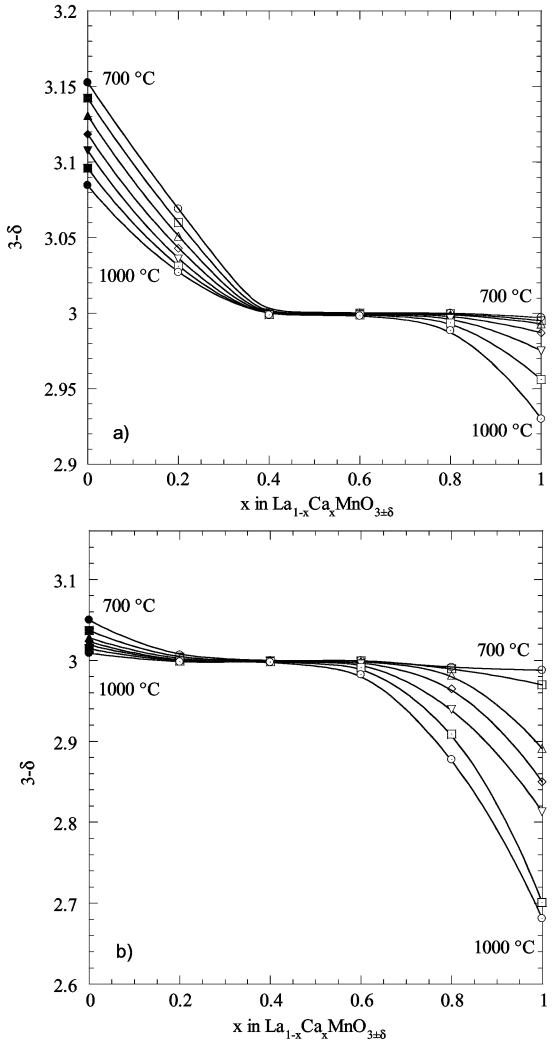

Fig. 3 Oxygen stoichiometry of $La_{1-x}Ca_xMnO_{3\pm\delta}$ between 700 and 1000 °C with steps of 50 °C. Filled symbols are literature data[44] and open symbols present data. Lines shown in the figure are guides to the eye. The TGA measurements were performed in a) air and b) N_2 (3×10^{-6} atm O_2).

Oxygen stoichiometry. The oxygen stoichiometry of the materials at room temperature was determined by iodometric titration combined with thermogravimetry. The data are given in Table 2. At 40 mol% Ca or higher all the compositions were stoichiometric within the uncertainty of the iodometric titration (3.00 ± 0.01). At low Ca-content the materials are oxygen excess or more precisely cation deficient.[15,36] The temperature dependence of the oxygen non-stoichiometry was further studied by thermogravimetry in air ($P_{O_2} = 0.21$ atm) and in flowing nitrogen ($P_{O_2} = 3 \times 10^{-6}$ atm). The data are shown as a function of the Ca-content in Fig. 3(a) and (b). High La-content gives cation deficiency ($\delta > 0$), while high Ca-content gives oxygen deficiency ($\delta < 0$). At intermediate substitution LCM is stoichiometric with respect to oxygen in the whole temperature range studied.

The LSM system ($0.0 < x \leqslant 1.0$)

Unit cell dimensions. The unit cell dimensions and crystal system of the LSM materials are given in Table 2. In the $La_{1-x}Sr_xMnO_{3\pm\delta}$ system ($0.2 \leqslant x \leqslant 1.0$) rhombohedral, tetragonal, and cubic perovskites were observed. $La_{0.8}Sr_{0.2}MnO_{3.06}$ and $La_{0.6}Sr_{0.4}MnO_{3.00}$ were rhombohedral, as previously reported.[22,23] $La_{0.4}Sr_{0.6}MnO_3$ adopted a tetragonal symmetry after annealing at 1400 °C. This was also reported by Kikuchi *et al.*,[3] but no unit cell dimensions or space group were given. Sundaresan *et al.*[37] reported that $La_{0.5}Sr_{0.5}MnO_{3-\delta}$ was tetragonal with space group *I*4/*mcm* and unit cell dimensions $a = b \approx \sqrt{2} \times a_p$ and $c \approx 2 \times a_p$. The X-ray pattern for $La_{0.4}Sr_{0.6}MnO_{3.00}$ could not be indexed with these settings. $Pr_{0.5}Sr_{0.5}MnO_3$ was found to be tetragonal with space group *F*4/*mmc*, which is a setting of *I*4/*mcm* with the same tilt system ($a^\circ a^\circ c^-$) and space group number (140).[38] The difference is given by the unit cell dimensions were $a = b \approx 2 \cdot a_p \neq c \approx 2 \times a_p$ for *F*4/*mmc*. With these settings $La_{0.4}Sr_{0.6}MnO_{3.00}$ was indexed as tetragonal with space group *F*4/*mmc*. $La_{0.2}Sr_{0.8}MnO_{3.00}$ and $SrMnO_{3.00}$ were found to be cubic, which is consistent with literature.[3,26]

The unit cell dimensions of LSM ($0.0 \leqslant x \leqslant 1.0$) are plotted in Fig. 4. The unit cell volumes of the stoichiometric materials ($x \leqslant 0.4$) show a near linear correlation with the degree of substitution, while the cation deficient (oxygen excess) materials $LaMnO_{3.16}$ and $La_{0.8}Sr_{0.2}MnO_{3.06}$ deviate from this linear relationship.

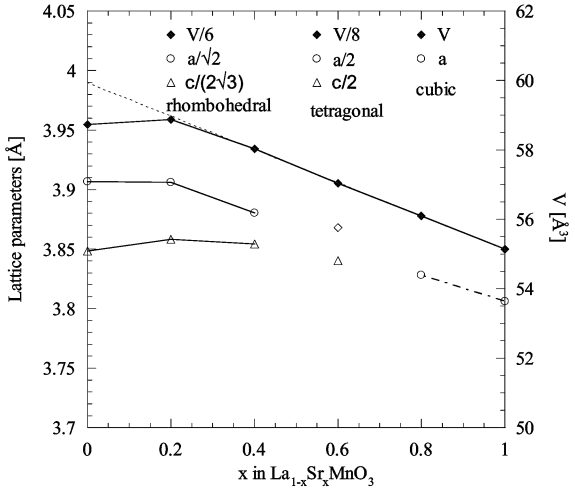

Fig. 4 Pseudocubic unit cell dimensions for the LSM system, rhombohedral ($x \leqslant 0.4$), tetragonal ($x = 0.6$) and cubic symmetry ($x \geqslant 0.8$) with increasing degree of Sr substitution. The unit cell parameters for materials with $x > 0.2$ are for metastable LSM. $La_{1-x}Sr_xMnO_3$ with $x = 0.4$, 0.6, 0.8, and 1.0 are stoichiometric, while materials with $x = 0.0$ and 0.2 have oxygen excess. The dashed line shows the linear relationship between the unit cell volume and the degree of substitution for stoichiometric samples.

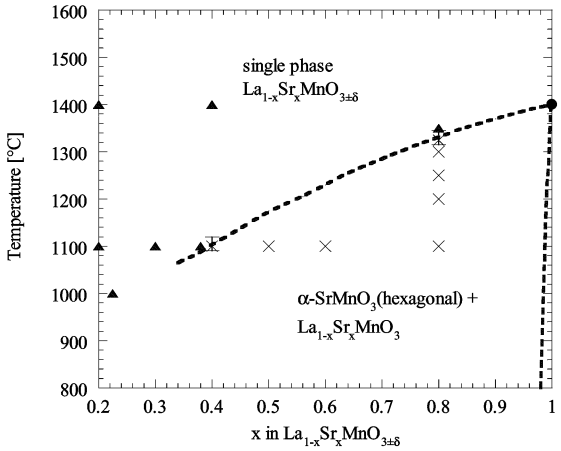

Fig. 5 Proposed phase diagram for the pseudo binary system $LaMnO_{3+\delta}$–$SrMnO_{3-\delta}$ in air. Filled triangles are single-phase materials with rhombohedral or cubic symmetry. Crosses are two-phase samples with the saturated LSM solid solution and the hexagonal α-$SrMnO_{3-\delta}$. The filled circle is the reported phase transition from hexagonal to perovskite $SrMnO_{3-\delta}$.[26]

Phase relations. The phase relation in the LSM system was studied by DTA/TGA and X-ray diffraction of materials annealed at various temperatures. The pseudo binary system $LaMnO_{3+\delta}$–$SrMnO_{3-\delta}$ at high $SrMnO_{3-\delta}$ content is shown in Fig. 5. The α–β $SrMnO_{3-\delta}$ phase transition at 1400 °C develops into a two-phase region separating the phase field for $La_{1-x}Sr_xMnO_{3\pm\delta}$ perovskite and hexagonal α-$SrMnO_{3-\delta}$. The two-phase region reported at 1100 °C in air by Cherepanov *et al.*[28] is adopted in Fig. 5. The phase composition for $La_{0.2}Sr_{0.8}MnO_{3\pm\delta}$ annealed at different temperatures was studied by XRD. A single-phase cubic perovskite was observed above 1330 ± 10 °C, while below a two-phase mixture of α-$SrMnO_{3-\delta}$ and $La_{1-x}Sr_xMnO_{3\pm\delta}$ perovskite were observed. The unit cell dimensions for the two phases as a function of annealing temperature are shown in Fig. 6. The cubic cell parameter for the perovskite decreases with increasing annealing temperature in line with increasing Sr-content. The unit cell parameters of α-$SrMnO_{3-\delta}$ changes with increasing annealing temperature in the two-phase region, and approaches those for pure α-$SrMnO_{3-\delta}$ annealed at 1350 °C (all samples were cooled at 600 °C h^{-1}). A low solubility of $LaMnO_{3+\delta}$ in α-$SrMnO_{3-\delta}$ is inferred from the fact that formation of α-$SrMnO_{3-\delta}$ from metastable $La_{1-x}Sr_xMnO_{3\pm\delta}$ solid solutions is slow.

DTA measurements on $La_{0.4}Sr_{0.6}MnO_{3\pm\delta}$ and $La_{0.2}Sr_{0.8}MnO_{3\pm\delta}$ gave broad endothermic peaks between 800 and 885 °C on heating to 1200 °C in air, and between 800 and 1100 °C in N_2 (*ca.* $\times 10^{-6}$ atm O_2), respectively. The materials were stoichiometric with respect to oxygen before and after the DTA measurement in air, and X-ray diffraction verified that the crystal structure had not changed as a result of the thermal treatment. Measurements under a gas flow of nitrogen changed the oxygen stoichiometry of $La_{0.4}Sr_{0.6}MnO_{3.00}$ and $La_{0.2}Sr_{0.8}MnO_{3.00}$ to 2.97 and 2.89, respectively. A change in the crystal structure was also verified by XRD, where the splitting of the *ca.* 33° 2θ peak disappeared for $La_{0.4}Sr_{0.6}MnO_{3-\delta}$ and appeared for $La_{0.2}Sr_{0.8}MnO_{3-\delta}$.

The α–β $SrMnO_{3-\delta}$ phase transition was investigated by DTA/TGA in a gas flow of both air and N_2, and the data are shown in Fig. 7(a) and (b). Cubic metastable $SrMnO_{3-\delta}$ is initially oxidised at 530 ± 5 °C, but reduction becomes predominant at 585 ± 5 °C. The phase transition from cubic to hexagonal $SrMnO_{3-\delta}$ is accompanied by an oxidation showing that α-$SrMnO_{3-\delta}$ is considerably more stoichiometric than metastable β-$SrMnO_{3-\delta}$. In N_2 the reduction of β-$SrMnO_{3-\delta}$ is initiated at 310 ± 5 °C. At the phase

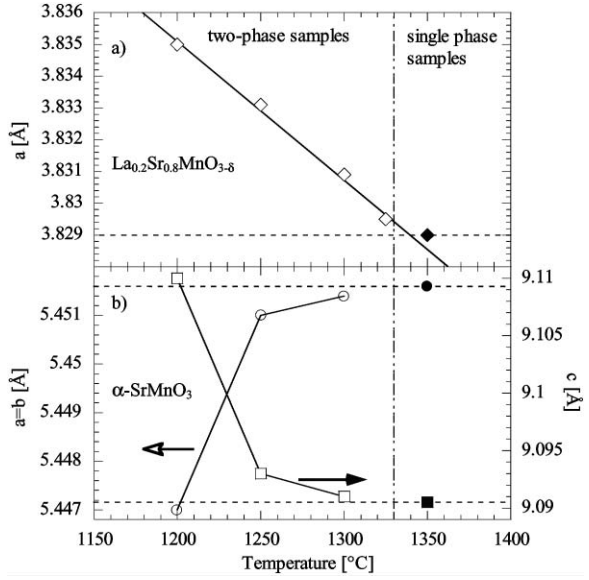

Fig. 6 a) Cubic lattice parameter for $La_{0.2}Sr_{0.8}MnO_{3-\delta}$. b) Hexagonal lattice parameters for α-$SrMnO_{3-\delta}$. Open symbols represent two-phase samples, while the filled symbols are single-phase samples. All samples were cooled at 600 °C h^{-1}.

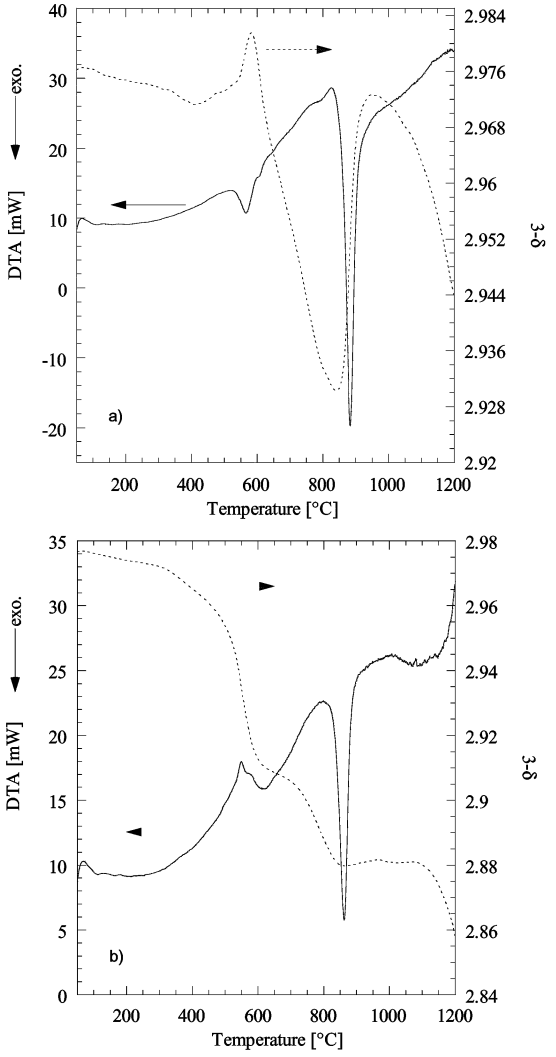

Fig. 7 DTA (solid line) and TGA (dotted line) curves for metastable perovskite $SrMnO_{2.98}$ heated in a gas flow of a) air and b) N_2. The first order phase transitions between the crystal modifications are shifted to lower T with higher δ (lower P_{O_2}).

transition the oxygen stoichiometry is nearly constant due to the formation of the stable α-$SrMnO_3$ phase. The α–β $SrMnO_{3-\delta}$ phase transition was initiated at 840 ± 10 and 825 ± 10 °C in air and N_2, respectively. The transition enthalpy was estimated to be 7.1 kJ mol^{-1} in air and 5.1 kJ mol^{-1} in N_2. The enthalpy of the phase transition was estimated by the following procedure: the enthalpy due to the simultaneous oxidation/reduction of the material was subtracted from/added to the measured enthalpy by using the measured mass loss and enthalpy of oxidation of $SrMnO_{3-\delta}$ reported by Rørmark *et al.*[30]

Oxygen stoichiometry. The oxygen stoichiometry of the LSM materials at room temperature was determined by iodometric titration combined with thermogravimetry. The data are given in Table 2. At 40 mol% Sr or higher all the compositions were stoichiometric within the uncertainty of the iodometric titration (3.00 ± 0.01) except for metastable cubic $SrMnO_{3-\delta}$. At low Sr-content the materials are cation deficient (oxygen excess). The temperature dependence of the oxygen non-stoichiometry was further studied by thermogravimetry in air ($P_{O_2} = 0.21$ atm) and in flowing nitrogen ($P_{O_2} = 3 \times 10^{-6}$ atm). The data are shown as a function of the Sr-content in Fig. 8(a) and (b). High La-contents give oxygen excess, while high Sr-contents give oxygen deficiency. At intermediate substitution LSM is stoichiometric with respect to oxygen in the whole temperature range studied. For metastable β-$SrMnO_{3-\delta}$ the oxygen non-stoichiometry was only measured at 700 °C, due to the formation of stable α-$SrMnO_3$ above 710 °C. The formation of α-$SrMnO_3$ was initiated between 710 and 720 °C in both air and N_2 (3×10^{-6} atm O_2). The formation of α-$SrMnO_3$ was confirmed by both oxidation (in air) and X-ray diffraction of β-$SrMnO_{3-\delta}$ annealed at 720 °C for 3–4 h. The oxygen non-stoichiometry for $750 \leqslant T \leqslant 1000$ °C, shown by crosses in Fig. 8(a) and (b), is interpolated from the present measurements and literature data for stable β-$SrMnO_{3-\delta}$ at $T \geqslant 1200$ °C.[26,27]

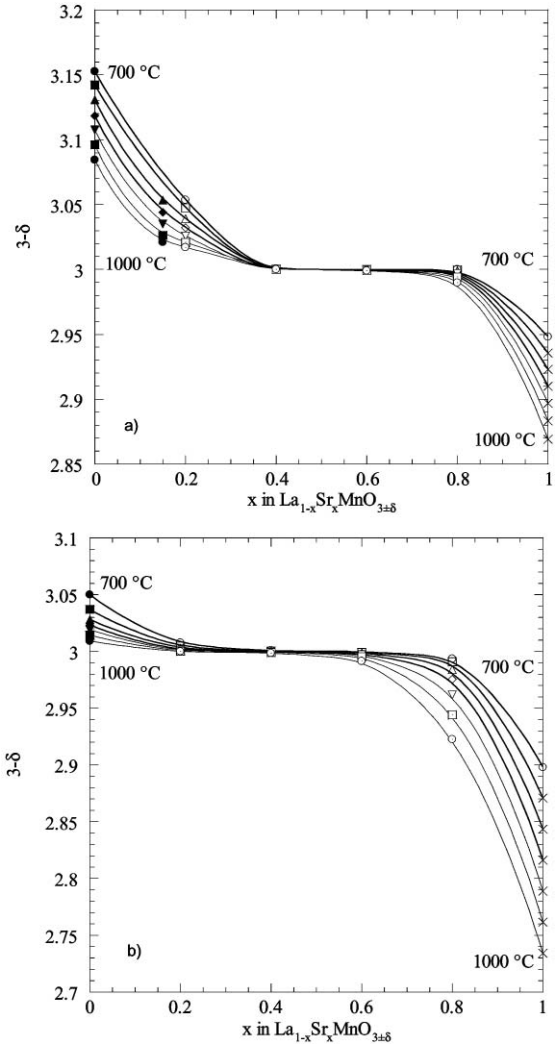

Fig. 8 Oxygen stoichiometry of $La_{1-x}Sr_xMnO_{3\pm\delta}$ between 700 and 1000 °C with steps of 50 °C. Filled symbols are literature data,[44] open symbols measured data, and crosses interpolated data from present measurements and literature data.[26,27] The lines are guides to the eye. Measurements were done in a) air and b) N_2 (3×10^{-6} atm O_2).

Discussion

The LCM system ($0.0 \leqslant x \leqslant 1.0$)

Unit cell parameters. The orthorhombic cell parameters shown in Fig. 1 are consistent with the literature data as shown in Fig. 1.[2] The unit cell parameters and the unit cell volume decrease with increasing x. All materials were stoichiometric except $LaMnO_{3.03}$ and $La_{0.8}Ca_{0.2}MnO_{3.07}$, which are cation deficient. The reduction in the unit cell volume is mainly due to the increasing amount of Mn^{4+}, which increases from 6% in pure $LaMnO_{3.03}$ to 100% in pure $CaMnO_{3.00}$ (ionic radii of 6 coordinated Mn^{4+} and Mn^{3+} are 0.53 and 0.645 (HS) Å, respectively[39]). The substitution of La with Ca also contributes to the shrinkage of the unit cell volume (ionic radii of 12 coordinated Ca^{2+} and La^{3+} are 1.34 and 1.36 Å respectively[39]). The exothermic enthalpy of formation of $La_{1-x}Ca_xMnO_3$ has been found to increase with increasing substitution of Ca.[32] This is mainly due to oxidation of Mn^{3+} to Mn^{4+}, which reflects shorter bond lengths due to the smaller ionic radii of Mn^{4+} and Ca^{2+} compared to Mn^{3+} and La^{3+} in accordance with the trends we found for the unit cell dimensions (Fig. 1).

The Goldschmidt tolerance factor $t = (r_A + r_O)/(\sqrt{2}(r_B + r_O))$ can be used to obtain information on the distortion of the perovskite lattice. r_A, r_B, and r_O are ionic radii of the A and B cations and the oxygen ion, respectively. Using the ionic radii from Shannon,[39] the calculated tolerance factors for $LaMnO_{3.0}$ and $CaMnO_{3.0}$ are 0.954 and 1.004, respectively. The coordination numbers used were 12 for La^{3+} and Ca^{2+} and 6 for Mn^{3+}, Mn^{4+}, and O^{2-}. The symmetry of the perovskite is expected to become more symmetric with increasing tolerance factor in accord with the unit cell parameters shown in Fig. 1.

The near linear relationship between cell parameters and Ca-content breaks down at low Ca-content due to Jahn–Teller distortion (Fig. 1). $LaMnO_{3.03}$ takes a Jahn–Teller distorted variant (ORT1) of the orthorhombic $GdFeO_3$-type structure.[12] The Jahn–Teller distortion also explains why the unit cell volume of $LaMnO_{3+\delta}$ is situated slightly above the linear relationship for the stoichiometric materials. The unit cell volume of $La_{0.8}Ca_{0.2}MnO_{3.07}$ is smaller than the linear relation found for the stoichiometric materials ($0.4 \leqslant x \leqslant 1.0$). The increasing Mn^{4+} concentration with increasing cation deficiency (oxygen excess) results in a contraction of the unit cell.

For LCM with $x > 0$ the a and c axes are almost equal (Table 2). From a study of interatomic distances and angles in LCM with $0.2 \leqslant x \leqslant 0.6$, fairly symmetrical MnO_6 octahedra were found.[2] The octahedra are tilted, and have the same orthorhombic structure as found for $LaMnO_{3+\delta}$ with intermediate amounts of Mn^{4+} (ORT2).[2,12]

Phase relations. Phase transitions were observed for both $CaMnO_{3-\delta}$ and $La_{0.1}Ca_{0.9}MnO_{3-\delta}$, see Fig. 2. There are only small discrepancies between our transition temperatures

and those reported by Taguchi *et al.*[18] However, the oxygen stoichiometry reported for $CaMnO_{3-\delta}$ by Taguchi *et al.* (2.65 and 2.56 at 900 and 920 °C, respectively) were far lower than those found in the present study (2.975 and 2.956 at 900 and 950 °C, respectively, see Fig. 3(a). Taguchi *et al.*[19] investigated also $Ca_{1-x}La_xMnO_{2.97}$ with $x = 0.05$–0.4. The phase transitions were only observed for $x = 0.05$ and 0.1 at 887 and 917 °C. Here, only a single endothermic peak at 914 °C was observed for $La_{0.1}Ca_{0.9}MnO_{3-\delta}$, while no transitions were observed for $La_{0.5}Ca_{0.5}MnO_{3-\delta}$ and $La_{0.8}Ca_{0.2}MnO_{3-\delta}$.

The reduction of Mn correlated with the phase transitions of $CaMnO_{3-\delta}$ and La substituted $CaMnO_{3-\delta}$ (see Fig 2.) raise the question whether the phase transitions are related to the oxygen non-stoichiometry. According to Gibbs phase rule, the maximum number of coexistent condensed phases in $CaMnO_{3-\delta}$ at a given partial pressure of oxygen is 2, and the solid–solid phase transition corresponds to an invariant point. Here, we have assumed that the Ca/Mn ratio is constant in both phases. This analysis supports that the transitions in $CaMnO_{3-\delta}$ are of first order, in line with the data shown in Fig. 2. The reduction in the phase transition temperature with increasing oxygen vacancy concentration is illustrated in Fig. 9. The temperature is constant when going through the two-phase region at constant partial pressure of oxygen.

In La substituted $CaMnO_{3-\delta}$, the number of components increases by one relative to $CaMnO_{3-\delta}$. Two coexisting condensed phases give one degree of freedom, and the solid–solid phase transitions of La substituted $CaMnO_{3-\delta}$ are no longer an invariant point according to the phase rule. The first order phase transition of La-substituted $CaMnO_{3-\delta}$ now occurs over a temperature range and should be more difficult to detect by DTA as shown for $La_{0.1}Ca_{0.9}MnO_{3-\delta}$ in Fig. 2. The compositional width of the two-phase region is expected to increase with increasing La-content, and the two-phase region is expected to shift to higher temperatures in line with the observation. Higher transition temperatures are expected due to the fact that the phase transition is associated with the increasing oxygen deficiency, which is shifted to higher temperatures with increasing La-content (Fig. 3). If sufficient cation mobility is present, the high temperature phase will nucleate and grow at the expense of the low temperature phase. The heat associated with the phase transition will therefore be consumed over a temperature interval that increases with increasing La-content. It is therefore reasonable that the DTA signature of the phase transition is strongly suppressed with increasing La-content in line with the present observations. Additional investigations (*i.e.* high temperature diffraction) are necessary in order to elucidate the two-phase regions in the LCM system at high Ca-content.

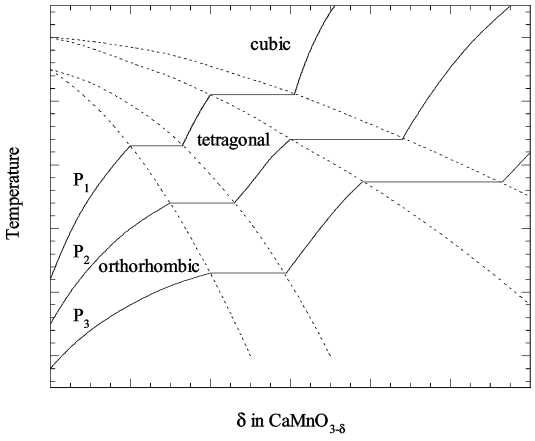

Fig. 9 Schematic illustration of the oxygen non-stoichiometry (δ) of $CaMnO_{3-\delta}$ as a function of temperature at constant partial pressure of oxygen. The partial pressure of oxygen is varying in the manner $P_1 > P_2 > P_3$.

No evidence for phase transitions of $LaMnO_{3.16}$ was observed by DTA up to 1350 °C in air. $LaMnO_{3+\delta}$ is found to tolerate both La excess and deficiency, $La_{1\pm x}MnO_{3+\delta}$.[40] However, assuming that the La/Mn ratio is not allowed to change during heating (low cation mobility), the Gibbs phase rule gives the same conditions as for $CaMnO_{3-\delta}$. At sufficiently high temperature the stoichiometric restriction (constant La/Mn-ratio) does not hold due to the possibility of cation diffusion. According to Gibbs phase rule two coexisting condensed phases does then give one degree of freedom. It is therefore reasonable that a mixture of orthorhombic and rhombohedral $LaMnO_{3+\delta}$ is observed by quenching materials annealed under certain conditions (inert or reducing atmosphere).[8–12] Similar two-phase mixtures of LSM materials have also been obtained by quenching experiments under various atmospheres.[25] In quenched samples the final oxygen content in the material decreases with increasing annealing temperature and decreasing partial pressure of oxygen. Rhombohedral structure is then found for high oxygen content, orthorhombic at low oxygen content and a two-phase mixture for intermediate oxygen content. The oxygen stoichiometry at 1000 °C is $LaMnO_{3.10}$ according to the present DTA/TGA measurement. This is close to the limit between rhombohedral and orthorhombic $LaMnO_{3+\delta}$ at room temperature. We therefore conclude that $LaMnO_{3+\delta}$ maintains rhombohedral symmetry in air up to 1350 °C. Reducing the oxygen partial pressure of oxygen to 10^{-5} atm is not sufficient to stabilise one of the orthorhombic structures as reported by Tagawa *et al.*[14]

No evidence for immiscibility near 50 mol% $LaMnO_3$ was observed in the LCM system, in contradiction to what was found by Majewski *et al.*[29] The complete miscibility is in accord with the linearly decreasing enthalpy of formation from the binary oxides with increasing Ca-content.[32] It is important to note in this context that orthorhombic $La_{1-x}Ca_xMnO_{3-\delta}$ is expected to transform to rhombohedral or tetragonal perovskite structure at elevated temperatures. Based on the analysis of the Gibbs phase rule presented above, the phase transitions are expected to be associated with two-phase regions, which may explain the observation by Majewski *et al.*[29] A careful mapping of these two-phase regions should be followed up in future investigations.

Oxygen stoichiometry. The LCM materials were apparently stoichiometric in the region around 40 mol% Ca in both air and N_2 (3×10^{-6} atm O_2), see Fig. 3(a) and (b). This is also illustrated in Fig. 10(a) and (b). The non-stoichiometry is given as the amount of Mn^{4+}, where the broken line along the diagonal of the figures represents stoichiometric materials. The enthalpy of formation of LCM from the binary oxides is found to increase linearly with increasing Ca-content.[32] The oxygen non-stoichiometry in LCM, which is fairly stoichiometric at intermediate degree of substitution, is therefore not determined by the Gibbs energy of formation of the stoichiometric perovskites as discussed in the following.

Pure $CaMnO_3$ is easily reduced (Fig. 3 and Fig. 10) leading to the formation of oxygen vacancies:

$$CaMnO_3 \rightleftharpoons CaMnO_{3-\delta} + \delta/2O_2(g) \quad (1)$$

or described by point defect equilibrium

$$O_O^x + 2Mn_{Mn}^x \rightleftharpoons V_O^{\bullet\bullet} + 2Mn'_{Mn} + 1/2O_2(g) \quad (2)$$

where O_O^x is oxygen in an oxygen site, Mn_{Mn}^x is Mn^{4+} in a Mn^{4+}-site, $V_O^{\cdot\cdot}$ is an oxygen vacancy, and Mn'_{Mn} is Mn^{3+} in a Mn^{4+}-site. On the other hand, pure $LaMnO_3$ is easily oxidised

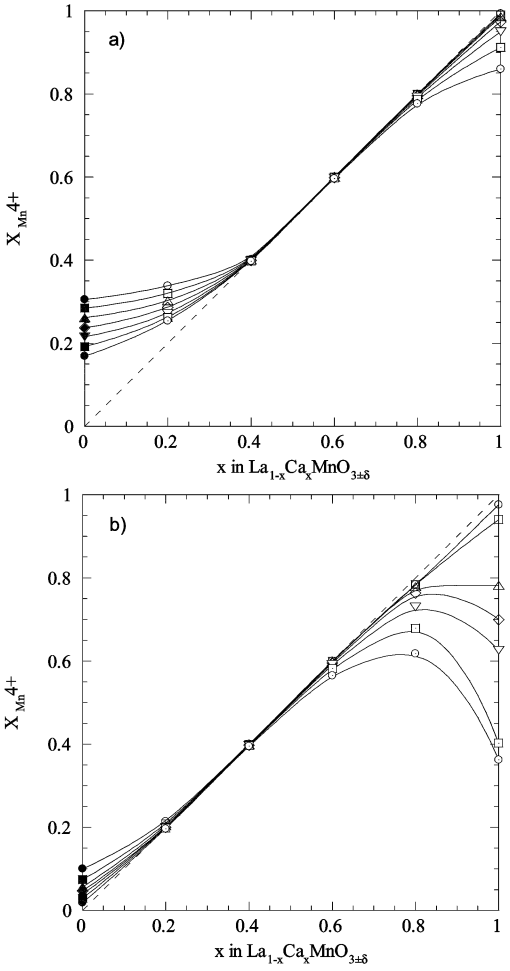

Fig. 10 The amount of Mn^{4+} as a function of x in $La_{1-x}Ca_xMnO_{3\pm\delta}$ between 700 and 1000 °C with steps of 50 °C. Filled symbols are literature data,[44] and open symbols are calculated from measured thermogravimetric data. Measurements were done in a) air and b) N_2 (3×10^{-6} atm O_2).

(Fig. 3 and Fig. 10) leading to the formation of equal amounts of La and Mn vacancies:

$$LaMnO_3+\delta/2O_2(g)\rightleftharpoons LaMnO_{3+\delta}\rightleftharpoons\frac{3+\delta}{3}La_{3/(3+\delta)}Mn_{3/(3+\delta)}O_3 \quad (3)$$

or described by point defect equilibrium

$$6Mn_{Mn}^{x}+3/2O_2(g)\rightleftharpoons V'''_{La}+V'''_{Mn}+6Mn_{Mn}^{\bullet}+3O_O^x \quad (4)$$

where Mn_{Mn}^{x} is Mn^{3+} in a Mn^{3+}-site, V''_{La} is a La vacancy, V'_{Mn} is a Mn vacancy, and $Mn_{Mn}^{\cdot}$ is Mn^{4+} in a Mn^{3+}-site. For the pure phases, $Ca_2Mn_2O_5$ (containing only Mn^{3+}) is obtainable,[20,35] while $LaMnO_{3.5}$ (containing only Mn^{4+}) has never been prepared. This shows that Mn^{3+} is more stable relative to Mn^{4+} for $CaMnO_{3-\delta}$ than Mn^{4+} relative to Mn^{3+} for $LaMnO_{3+\delta}$. The enthalpy of reduction of $CaMnO_3$ is positive,[30] while the enthalpy of oxidation of $LaMnO_3$ is negative.[32] Substituting La for Ca in $CaMnO_3$ increases the endothermic enthalpy of reduction as demonstrated by the decreasing oxygen non-stoichiometry (Fig. 3). On the other hand, substituting Ca for La in $LaMnO_3$ decreases the exothermic enthalpy of oxidation as shown by the decreasing oxygen excess with increasing Ca-content (Fig. 3). Reaction (3) is completely shifted to the right at around 40 mol% Ca. At this Ca concentration and higher the enthalpy of oxidation, eqn. (3), has become small or even endothermic. The LCM materials are therefore most stoichiometric both with respect to oxygen excess and deficiency at intermediate Ca-content (40–50 mol% Ca).

Special attention should be given to the $CaMnO_{3-\delta}$ sample measured in 3×10^{-6} atm O_2. Two phase transitions are seen, where the non-stoichiometry changes drastically in a step of 50 °C. The change is seen between 750 and 800 °C and between 900 and 950 °C (Fig. 3(b) and Fig. 10(b)). The first transition appears in the same oxygen non-stoichiometry range as the phase transitions seen for measurements in air, but at a lower temperature. This agrees with the assumption that a decrease in oxygen partial pressure will reduce the temperature for the phase transition due to the association between vacancy concentration and phase transition. The second transition may be due to the formation of an ordered reduced $CaMnO_{3-\delta}$ phase, but the order–disorder transitions or the homogeneity regions for these reduced phases are not known.[41]

The LSM system ($0.0 < x \leqslant 1.0$)

Unit cell dimensions. The unit cell volume increases from $LaMnO_{3.16}$ to $La_{0.8}Sr_{0.2}MnO_{3.06}$, and then decreases with increasing x (Fig. 4). The amount of Mn^{4+} is 32% in both $LaMnO_{3.16}$ and $La_{0.8}Sr_{0.2}MnO_{3.06}$. The Mn^{4+} concentration increases further continuously to 100% in $SrMnO_{3.00}$. The higher unit cell volume of $La_{0.8}Sr_{0.2}MnO_{3.06}$ compared to $LaMnO_{3.16}$ is explained by the substitution of the bigger Sr ion in place of La ions, equal amounts of Mn^{4+} in both compounds, and the higher cation deficiency (oxygen excess) for $LaMnO_{3.16}$. The reduction of the unit cell volume from $x \geqslant 0.2$ demonstrates that the increasing concentration of Mn^{4+} is far more important for the unit cell volume than the substitution of La with Sr. The decrease in the unit cell volume is less in LSM than in LCM, see Fig. 1 and Fig. 4, which is expected since Ca^{2+} is smaller than Sr^{2+}.[39]

The Goldschmidt tolerance factor for $LaMnO_{3.0}$ and $SrMnO_{3.0}$ is 0.954 and 1.041, respectively (ionic radii:[39] Sr^{2+} and La^{3+}, CN = 12; 1.44 and 1.36 Å, Mn^{4+} and Mn^{3+}, CN = 6: 0.53 and 0.645 (HS)). The cubic symmetry found for high Sr-content is therefore in line with the increasing tolerance factor with increasing Sr-content.

The enthalpy of formation of stoichiometric LSM becomes more exothermic with increasing Sr-substitution.[32] This is mainly due to oxidation of Mn^{3+} to Mn^{4+}, which reflects shorter bond lengths due to the smaller ionic radii of Mn^{4+} compared to Mn^{3+} as in the case of the LCM system.

Phase relations. The transition of the metastable cubic β-$SrMnO_{3-\delta}$ to the stable hexagonal α-$SrMnO_{3-\delta}$ in air was found, by Negas and Roth,[26] not to involve oxidation. DTA/TGA measurements of β-$SrMnO_{2.98}$ (Fig. 7(a)) demonstrate that β-α $SrMnO_{3-\delta}$ transition indeed involves an oxidation. In air β-$SrMnO_{3-\delta}$ is reduced prior to the transition, while an oxidation occurs during the transition since the oxygen vacancy concentration in α-$SrMnO_{3-\delta}$ is not significant before 950 ± 10 °C. In N_2 (Fig 7(b)) only reduction of β-$SrMnO_{3-\delta}$ occurred prior to the phase transition. The oxygen stoichiometry becomes nearly constant in certain temperature intervals (600–700 °C, $3-\delta \approx 2.91$ and 850–1150 °C, $3-\delta \approx 2.88$). A possible explanation for this behaviour is the formation of phases with ordered oxygen vacancies. The β–α $SrMnO_{3-\delta}$ transition involves no change in the oxygen stoichiometry in pure N_2 as no oxygen is available for oxidation. The enthalpy of the perovskite to hexagonal transition in $SrMnO_{3-\delta}$ was estimated to be −7.1 and −5.1 kJ mol^{-1} in air and N_2, respectively. The transition enthalpy found for $SrMnO_{3-\delta}$ is in good accord with the transition enthalpy of $BaTiO_3$(perovskite) to $BaTiO_3$(hexagonal) from solution calorimetry, which was found to be 5.6 ± 3.4 kJ mol^{-1}.[42]

The present investigation has shown that the crystal

structure of LSM perovskites is sensitive to both oxygen non-stoichiometry and the level of Sr-substitution. According to the discussion of the Gibbs phase rule in relation to the LCM system, it is clear that a first order transition between two LSM phases with different crystal structures is expected to be associated with two-phase regions. DTA in air on LSM with $x = 0.6$ and 0.8 showed broad endothermic peaks on heating and no peaks on cooling but no structural difference was observed by XRD after the measurement. High temperature X-ray diffraction is necessary in order to find out if the endothermic events are associated with a two phase region separating LSM materials with different symmetry. The DTA measurements in N_2 showed broader peaks than in air. In addition the oxygen stoichiometry was reduced and the crystal structure had changed during the thermal cycling. The structural change is probably related to the increased oxygen vacancy concentration.

Based on the present findings and previous investigations,[28] the two-phase region between LSM perovskite and hexagonal α-$SrMnO_{3-\delta}$ has been established. At temperatures below 1000 °C LSM with $x \sim 0.3$ or higher is metastable with respect to hexagonal α-$SrMnO_{3-\delta}$ and LSM with lower content of Sr (Fig. 5). This is of particular importance for application of LSM in solid oxide fuel cells. In this respect it is fortunate that the solubility of α-$SrMnO_{3-\delta}$ in LSM is increasing with decreasing partial pressure of oxygen.[28] Based on the present investigation it is shown that the crystal structure of metastable LSM changes from rhombohedral to tetragonal to cubic with increasing Sr-content. The precipitation of stable α-$SrMnO_{3-\delta}$ from metastable LSM solid solution is slow, probably due to the low solubility of La in α-$SrMnO_{3-\delta}$ (Fig. 5).

Oxygen stoichiometry. The LSM materials were apparently stoichiometric in the region around 40 mol% Sr in both air and N_2 (310^{-6} atm O_2), see Fig. 8(a) and (b). This is also illustrated in Fig. 11(a) and (b). The non-stoichiometry is given as the amount of Mn^{4+}, where the broken lines along the diagonal of the figures represent stoichiometric materials. Mizusaki *et al.*[43] have measured the oxygen non-stoichiometry of $La_{1-x}Sr_xMnO_{3\pm\delta}$ with $x = 0.1$, 0.2, 0.3, 0.4, and 0.5. These results support that $La_{0.6}Sr_{0.4}MnO_3$ and $La_{0.5}Sr_{0.5}MnO_3$ are near stoichiometric at both 0.21 atm and 3×10^{-6} atm O_2, and that the oxygen excess increases from $La_{0.7}Sr_{0.3}MnO_3$ to pure $LaMnO_{3+\delta}$. As for LCM, the enthalpy of formation of LSM is found to increase with increasing Sr-content.[32] The defect chemistry of LSM can be explained by the two reactions (1) and (3) given previously for LCM. The endothermic enthalpy of reaction (1), where Sr replaces Ca, increases with increasing Sr-content. The exothermic enthalpy of reaction (3) decreases with increasing Sr substitution in line with arguments presented in the case of the LCM materials.

Conclusions

The present work has shown that orthorhombic $LaMnO_{3+\delta}$ and $CaMnO_{3-\delta}$ form a stable solid solution in the whole composition region. In contrast $SrMnO_{3-\delta}$, which forms a hexagonal structure of face sharing octahedra, is only partly soluble in $LaMnO_{3+\delta}$, and the solubility is strongly temperature dependent. Above 1400 °C, where the transition of hexagonal to perovskite $SrMnO_{3-\delta}$ occurs, perovskite $La_{1-x}Sr_xMnO_{3-\delta}$ solid solutions are stable in the whole concentration region. Metastable perovskite $La_{1-x}Sr_xMnO_{3-\delta}$ with high Sr-content may easily be prepared due to slow nucleation of hexagonal α-$SrMnO_3$. The crystal structure of metastable $La_{1-x}Sr_xMnO_{3-\delta}$ varies from rhombohedral, tetragonal to cubic, but the stability regions for these are still not established. The unit cell volume of the solid solutions

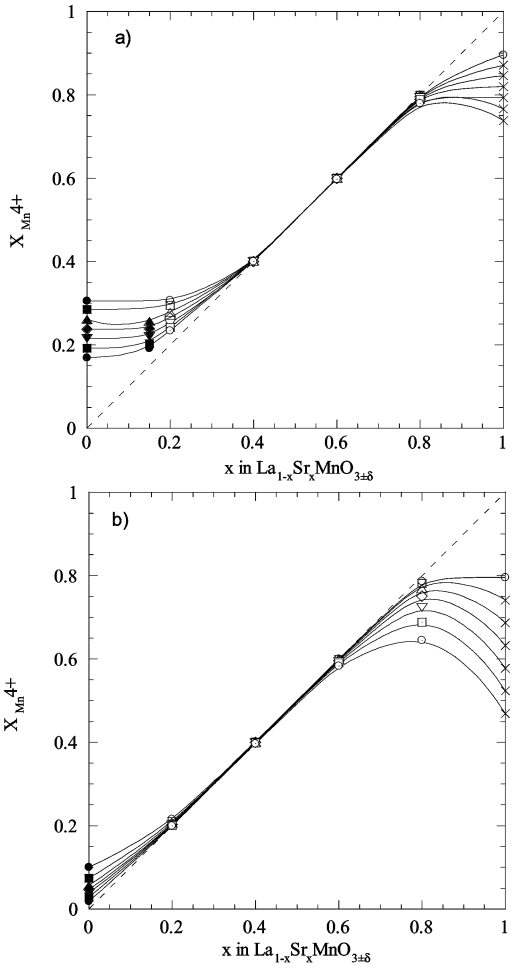

Fig. 11 The amount of Mn^{4+} as a function of x in $La_{1-x}Sr_xMnO_{3\pm\delta}$ between 700 and 1000 °C with steps of 50 °C. Filled symbols are literature data,[44] open symbols are calculated from measured thermogravimetric data, and crosses are values interpolated from present measurements and literature data.[26,27] Measurements were done in a) air and b) N_2 (3×10^{-6} atm O_2).

$La_{1-x}Ca_xMnO_{3\pm\delta}$ and $La_{1-x}Sr_xMnO_{3\pm\delta}$ decreases nearly linearly with decreasing La-content mainly due to the transformation from Mn^{3+} to Mn^{4+}. At high La-content the solid solutions are cation deficient (oxygen excess) relative to the ideal perovskite stoichiometry, while at low La-content and elevated temperature the materials are oxygen deficient.

Acknowledgement

Financial support from the Research Council of Norway is acknowledged.

References

1 B. Dabrowski, R. Dybzinski, Z. Bukowski, O. Chmaissem and J. D. Jorgensen, *J. Solid State Chem.*, 1999, **146**, 448.
2 S. Faaland, K. D. Knudsen, M. A. Einarsrud, L. Rørmark, R. Høier and T. Grande, *J. Solid State Chem.*, 1998, **140**, 320.
3 K. Kikuchi, H. Chiba, M. Kikuchi and Y. Syono, *J. Solid State Chem.*, 1999, **146**, 1.
4 A. A. Mukhin, V. Y. Ivanov, V. D. Travkin, S. P. Lebedev, A. Pimenov, A. Loidl and A. M. Balbashov, *JETP Lett.*, 1998, **68**, 356.
5 P. G. Radaelli, D. E. Cox, M. Marezio, S. -W. Cheong, P. E. Schiffer and A. P. Ramirez, *Phys. Rev. Lett.*, 1995, **75**, 4488.
6 A. Urushibara, Y. Moritomo, T. Arima, A. Asamitsu, G. Kido and Y. Tokura, *Phys. Rev. B*, 1995, **51**, 14103.
7 P. Schiffer, A. P. Ramirez, W. Bao and S. W. Cheong, *Phys. Rev. Lett.*, 1995, **75**, 3336.

8 A. K. Bogush, V. I. Pavlov and L. V. Balyko, *Cryst. Res. Technol.*, 1983, **18**, 589.
9 J. A. M. van Roosmalen, P. van Vlaanderen, E. H. P. Cordfunke, W. L. Ijdo and D. J. W. Ijdo, *J. Solid State Chem.*, 1995, **114**, 516.
10 J. Töpfer, J. P. Doumerc and J. C. Grenier, *J. Mater. Chem.*, 1996, **6**, 1511.
11 J. Töpfer and J. B. Goodenough, *J. Solid State Chem.*, 1997, **130**, 117.
12 B. C. Hauback, H. Fjellvåg and N. Sakai, *J. Solid State Chem.*, 1996, **124**, 43.
13 N. Sakai and H. Fjellvåg, *Acta Chem. Scand.*, 1996, **50**, 580.
14 H. Tagawa, J. Mizusaki, H. Nambu, C. Nakao, H. Takai and H. Minamiue, *Br. Ceram. Proc.*, 1996, **56**, 113.
15 J. A. M. van Roosmalen, E. H. P. Cordfunke, R. B. Helmholdt and H. W. Zandbergen, *J. Solid State Chem.*, 1994, **110**, 100.
16 Y. Murakami, D. Shindo, H. Chiba, M. Kikuchi and Y. Syono, *J. Solid State Chem.*, 1998, **140**, 331.
17 H. Taguchi, *J. Solid State Chem.*, 1996, **124**, 360.
18 H. Taguchi, M. Nagao, T. Sato and M. Shimada, *J. Solid State Chem.*, 1989, **78**, 312.
19 H. Taguchi and M. Shimada, *J. Solid State Chem.*, 1986, **63**, 290.
20 K. R. Poeppelmeier, M. E. Leonowicz and J. M. Longo, *J. Solid State Chem.*, 1982, **44**, 89.
21 A. Hammouche, E. Siebert and A. Hammou, *Mat. Res. Bull.*, 1989, **24**, 367.
22 I. G. Krogh Andersen, E. Krogh Andersen, P. Norby and E. Skou, *J. Solid State Chem.*, 1994, **113**, 320.
23 R. Millini, M. F. Gagliardi and G. Piro, *J. Mater. Sci.*, 1994, **29**, 4065.
24 Y. Takeda, S. Nakai, T. Kojima, R. Kanno, N. Imanishi, G. Q. Shen, O. Yamamoto, M. Mori, C. Asakawa and T. Abe, *Mat. Res. Bull.*, 1991, **26**, 153.
25 J. F. Mitchell, D. N. Argyriou, C. D. Potter, D. G. Hinks, J. D. Jorgensen and S. D. Bader, *Phys. Rev. B*, 1996, **54**, 6172.
26 T. Negas and R. S. Roth, *J. Solid State Chem.*, 1970, **1**, 409.
27 K. Kuroda, K. Shinozaki, K. Uematsu, N. Mizutani and M. Kato, *J. Am. Ceram. Soc.*, 1980, **63**, 109.
28 V. A. Cherepanov, L. Y. Barkhatova and V. I. Voronin, *J. Solid State Chem.*, 1997, **134**, 38.
29 P. Majewski, L. Epple, M. Rozumek, H. Schluckwerder and F. Aldinger, *J. Mater. Res.*, 2000, **15**, 1161.
30 L. Rørmark, K. Wiik, S. Stølen and T. Grande, *Chem. Mater*, 2001, **13**, 4005.
31 L. Rørmark, R. Stevens, J. Boerio-Goates, K. Wiik, S. Stølen and T. Grande, in preparation.
32 L. Rørmark, K. Wiik, S. Stølen and T. Grande, *J. Solid State Chem.*, in press.
33 G. H. Jonker and J. H. van Santen, *Physica*, 1950, **16**, 337.
34 N. Sakai, H. Fjellvåg and B. Lebech, *Acta Chem. Scand.*, 1997, **51**, 904.
35 K. R. Poeppelmeier, M. E. Leonowicz, J. C. Scanlon and J. M. Longo, *J. Solid State Chem.*, 1982, **45**, 71.
36 J. A. M. van Roosmalen and E. H. P. Cordfunke, *J. Solid State Chem.*, 1994, **110**, 106.
37 A. Sundaresan, P. L. Paulose, R. Mallik and E. V. Sampathkumaran, *Phys. Rev. B*, 1998, **57**, 2690.
38 D. N. Argyriou, D. G. Hinks, J. F. Mitchell, C. D. Potter, A. J. Schultz, D. M. Young, J. D. Jorgensen and S. D. Bader, *J. Solid State Chem.*, 1996, **124**, 381.
39 R. D. Shannon, *Acta Crystallogr., Sect. A*, 1976, **32**, 751.
40 J. Töpfer and J. B. Goodenough, *Chem. Mater.*, 1997, **9**, 1467.
41 A. Reller, J. M. Thomas, D. A. Jefferson and M. K. Uppal, *Proc. R. Soc. Lond., Ser. A*, 1984, **394**, 223.
42 E. Takayama-Muromachi and A. Navrotsky, *J. Solid State Chem.*, 1988, **72**, 244.
43 J. Mizusaki, N. Mori, H. Takai, Y. Yonemura, H. Minamiue, H. Tagawa, M. Dokiya, H. Inaba, K. Naraya, T. Sasamoto and T. Hashimoto, *Solid State Ionics*, 2000, **129**, 163.
44 J. A. M. van Roosmalen and E. H. P. Cordfunke, *J. Solid State Chem.*, 1994, **110**, 109.